Journal of Computational Electronics (2021) 20:900–911
https://doi.org/10.1007/s10825-020-01632-0

Waveguide divider design based on null of electric field

Leonardo Zappelli[1]

Received: 18 September 2020 / Accepted: 28 November 2020 / Published online: 19 January 2021

Abstract
Nowadays, the design of dividers is based on electromagnetic software that optimizes some geometric parameters to obtain the required performance. The choice of the geometry of the discontinuities contained in the divider and of the optimization initial point is quite critical to satisfy the divider requirements. In the last years, it is quite rare to find in the literature a theoretical approach helping the designers in the choice of the divider geometry. Helpful suggestion can derive by the analysis of the electric field in a trial divider that satisfies power division among the output ports in a thin band. In fact, the electric field null can be filled with metallic septa that ensure the same behavior at any frequency. The optimization of the septa position/form with numerical electromagnetic software permits to obtain divider with large bandwidth. A further analysis of the electric field null in the divider permits to add lateral metallic septa that further enlarge the transmission band. Finally, the design of an input matching network increases the transmitted power to the desired value.

Keywords Dividers · Waveguide · Beam forming network · Equivalent circuits · Passive components

1 Introduction

Waveguide dividers and couplers have been studied since '40s. Typical examples are Riblet's coupler, Bethe coupler, Wilkinson coupler [1–3]. These kinds of devices are based on fine and winning theoretical approaches. Nowadays, theoretical approaches to the study of couplers and dividers are quite rare [4–6], being replaced by "black box" approaches based on numerical software as CST, HFSS and others [7–14]. These softwares are able to design devices by means of an optimization of the geometrical parameters of a trial device until the desired functional is minimized. Usually, the functional is related to the performance required by the device, as the minimization of reflection and equi-amplitude of the output power, in case of dividers. Many examples of dividers based on this approach are discussed in the literature, and they can be divided in two classes. The first analyzes couplers based on top coaxial input that feeds output ports usually distributed along a ring [4–6] while the second is based on dividers designed in the E or H plane where an input port feeds the opposite output ports. These dividers can be based on Riblet's theory [9, 12], where insulated ports are closed on matched waveguide, or Bagley's theory [14] or other approaches based on the interactions between discontinuities to obtain power division [8, 10, 13].

In the designs that require use of simulation software, the main problem in finding the solution is the choice of the initial point for the geometrical optimization. In fact, the probability to incur in local minimum is strictly related to the starting point of the optimization. Hence, this choice is quite important to obtain the required performance for the device under study.

This paper focuses on equi-amplitude 1:N waveguide dividers, starting from a theoretical circuit approach that permits to obtain a single-frequency divider satisfying the required performances. Obviously, this divider has a thin bandwidth, but it contains a fundamental information to design a larger bandwidth divider. In fact, this trial divider is used to find the positions where the electric field vanishes in the divider core. These positions are filled with central metallic septa that ensure electric field null for any frequency, enlarging the bandwidth of the trial divider. A further analysis of the electric field in the divider core with central septa permits to understand the placement of lateral septa that further enlarge the bandwidth. The final stage is the design of a matching network that increases the power

✉ Leonardo Zappelli
l.zappelli@univpm.it

[1] Dipartimento di Ingegneria dell'Informazione, Università Politecnica delle Marche, Via Brecce Bianche, 60131 Ancona, Italy

transmitted to each output port to the theoretical maximum value for a lossless divider, $10\log_{10}(\frac{1}{N})$ dB, where N is the number of the output ports.

2 Theory

The goal is the design of H-plane waveguide equi-amplitude 1:3 divider ($|S_{11}| = 0, |S_{21}| = |S_{31}| = |S_{41}| = \frac{1}{\sqrt{3}}$ or -4.77 dB) with a band of 10% centered at 10 GHz. Many realizations of the divider could be proposed and, for example, a possible realization is shown in Fig. 1, which is formed by the divider core, where the electromagnetic field interacts with divider ports yielding to power division between outputs, and an input matching network that ensures matching and maximum power transfer to the divider core and, indirectly, to the output ports. The divider is represented by a 4×4 scattering matrix S where the terms S_{k1}, $k = 2,3,4$ represent the transmission toward the output ports when the first port is excited. The simplest configuration of the divider shown in Fig. 1, i.e., the empty divider without iris ($w_{\text{iris}} = a$), does not satisfy the required power division and an optimization of h_t does not permit to reach this goal.

Anyway, there is a very fast approach to reach the required power division among the output ports also for this structure. The approach is similar to that used in [15] to design four and six-ports hybrid couplers. In fact, the required power division can be obtained placing a proper iris at port 3 (central output port). In fact, as discussed in [16], a divider can be represented with a four-port equivalent circuit based on a polygon with four normalized susceptances placed at sides ($b_{12}, b_{23}, b_{34}, b_{14}$) and two susceptances on the diagonals (b_{13}, b_{24}). Moreover, four input transmission lines of electrical length $\theta_1, \theta_2, \theta_3, \theta_4$ connect each side to the actual four ports of the device, as shown in Fig. 2. The susceptances are normalized to the modal impedance of the TE_{10} mode by the transformers. Once the equivalent circuit has been defined, and setting $b_{23} = b_{14}$ and $b_{13} = b_{24}$ by symmetry, we can evaluate the particular value of the susceptance b_{34} that satisfies $|S_{21}| = |S_{31}| = |S_{41}|$. With simple circuit/mathematical manipulations, we can write the first column of the scattering matrix of the divider as:

$$|S_{k1}| = \frac{1}{\Delta}\begin{bmatrix} N_{11} \\ N_{21} \\ N_{31} \\ N_{21} \end{bmatrix} \tag{1}$$

with

$$N_{21} = \left(2b_{13} + b_{14} + b_{34}\right)^2 \tag{2}$$

$$+ \left[-1 + b_{14}b_{34} + b_{13}(b_{13} + b_{14} + b_{34})\right]^2 \tag{3}$$

$$N_{31} = 4b_{14}^2 + \left(1 + b_{13}^2 - b_{14}^2\right)^2 \tag{4}$$

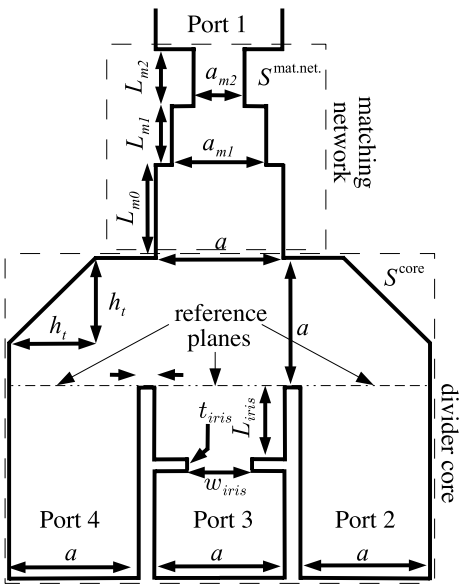

Fig. 1 1:3 WR90 waveguide empty divider

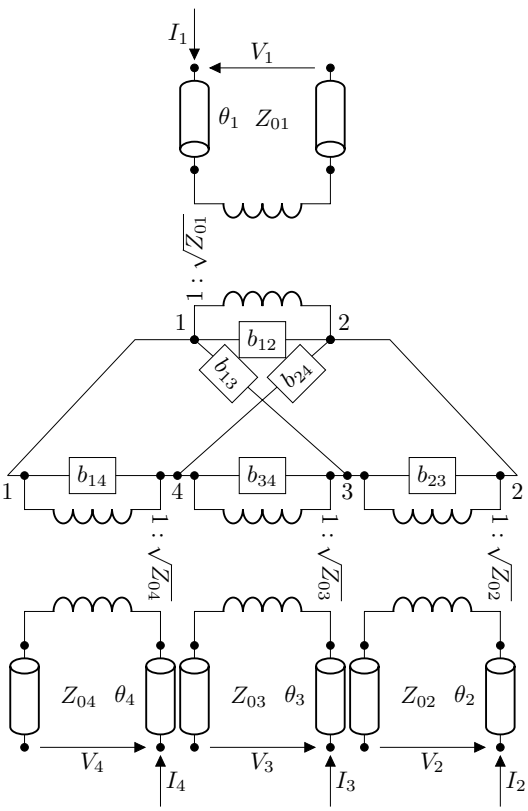

Fig. 2 Equivalent circuit for the four-port divider shown in Fig. 1

N_{11} is not reported because its knowledge is not important at this stage and Δ is the real denominator of $|S_{k1}|$. The key to obtain an equi-amplitude divider is to impose $N_{21} = N_{31}$, obtaining two possible solutions:

$$b_{34} = -b_{14} \tag{5}$$

$$b_{34} = b_{14} - 2b_{13}. \tag{6}$$

These solutions permit to design a trial divider, placing an iris at a proper distance from the third port, to change the global value of b_{34} in order to satisfy (5) or (6) [15].

In fact, the equivalent circuit of the empty core divider shown in Fig. 1, without iris and matching network ($w_{\text{iris}} = a, a_{m1} = a_{m2} = a$), can be easily identified solving four polynomial equations that permit to obtain the values of the four transmission lines lengths θ_i^{empty}, $i = 1, 2, 3, 4$ and, then, the six susceptances b_{ij}^{empty} with simple circuit manipulations [16]. Hence, the scattering matrix of the empty core divider at the reference planes, S^{empty}, can be numerically evaluated by CST at 10 GHz for $s = 3, a = 22.86$ (dimensions are in mm throughout the paper), and it can be used to identify the elements of the equivalent circuit shown in Fig. 2, characterized by: $b_{12}^{\text{empty}} = -0.962$, $b_{23}^{\text{empty}} = b_{14}^{\text{empty}} = -0.881, b_{34}^{\text{empty}} = -0.774, b_{13}^{\text{empty}} = b_{24}^{\text{empty}} = 1.321$, $\theta_1^{\text{empty}} = 10.2°, \theta_2^{\text{empty}} = \theta_4^{\text{empty}} = 7.5°, \theta_3^{\text{empty}} = 4.7°$. As previously discussed, equi-amplitude division is not obtained with the empty divider, but the presence of an iris at a proper distance from port 3, as shown in Fig. 1, could permit to reach the required goal.

In fact, if we choose an iris with susceptance $b_{\text{iris}} = -b_{14}^{\text{empty}} - b_{34}^{\text{empty}} = 0.881 + 0.774 = 1.655$, satisfying (5), we could reach the required power division if we put the iris at a distance $\theta_{\text{iris}} = 180° - \theta_3^{\text{empty}} = 175.3°$ from the reference plane of the third port. This distance ensures that the iris susceptance b_{iris} is in shunt with b_{34}^{empty}, obtaining a total susceptance at port 3 equal to $b_{34}^{\text{tot}} = b_{\text{iris}} + b_{34}^{\text{empty}} = -b_{14}^{\text{empty}} - b_{34}^{\text{empty}} + b_{34}^{\text{empty}} = -b_{14}^{\text{empty}}$, satisfying (5). Now, we must choose the iris dimensions to synthesize the obtained value for b_{iris}. The first choice should be to select a capacitive iris, with vertical diaphragms, but this would require a global divider in the H-plane with an iris in the E-plane. Our goals is to obtain a divider in the H-plane, and the desired susceptance b_{iris} can be realized with an inductive iris with value $-b_{\text{iris}}$, surrounded by two lines of lengths $\theta_{\text{rev}} = -\arctan\left(2/b_{\text{iris}}\right) = 50.4°$ and $180° - \theta_{\text{rev}}$ [15]. Hence, the distance of the inductive iris from the third input port is: $\theta_{\text{iris}} = 180° - \theta_3^{\text{empty}} - \theta_{\text{rev}} = 124.9° = 2.18\,\text{rad} = \beta L_{\text{iris}} = \frac{2\pi}{\lambda_g} L_{\text{iris}}$ which corresponds to $L_{\text{iris}} = 13.78$ mm. Finally, the width of the iris is obtained by a simple evaluation [2], obtaining $w_{\text{iris}} = 11.61$ mm with thickness $t = 0.2$ mm.

With the chosen iris, the required power division ($\left|S_{21}^{\text{core}}\right| = \left|S_{31}^{\text{core}}\right|$) is reached at 10 GHz, as shown in Fig. 3a where $\left|S_{11}^{\text{core}}\right|$, $\left|S_{21}^{\text{core}}\right|$, $\left|S_{31}^{\text{core}}\right|$ are reported with red lines (left axis) and the difference $\left|S_{21}^{\text{core}}\right|_{\text{dB}} - \left|S_{31}^{\text{core}}\right|_{\text{dB}}$ with blue dashed starred line (right axis). $\left|S_{11}^{\text{core}}\right|$ is less than −8 dB, while the transmission band, chosen as the band where $-0.2\,\text{dB} \le \left|S_{21}^{\text{core}}\right|_{\text{dB}} - \left|S_{31}^{\text{core}}\right|_{\text{dB}} \le 0.2\,\text{dB}$, is about 600 MHz (9.5÷10.1), less than required and not centered at 10 GHz. Though requirements are not satisfied, we end this divider design putting an optimized matching network, based on $\lambda_g/4$ transformers, at the input port to maximize transmission power to the output ports, as shown in Fig. 1 ($L_{m0} = 9.8$, $L_{m1} = 16$, $L_{m2} = 14.85$, $a_{m1} = 16.86$, $a_{m2} = 17.66$). The final divider scattering parameters are shown in Fig. 3a with black lines ($\left|S_{11}^{\text{div}}\right|$, $\left|S_{21}^{\text{div}}\right|$, $\left|S_{31}^{\text{div}}\right|$). It is obvious and evident that the matching network does not alter the transmission band if the distance L_{m0} is properly chosen, as it can be deduced comparing the difference $|S_{21}|_{\text{dB}} - |S_{31}|_{\text{dB}}$ in both cases (matched divider, green, or divider core, blue). Reflection decreases (lower than −20 dB) and $\left|S_{21}^{\text{div}}\right|$, $\left|S_{31}^{\text{div}}\right|$ increase to the desired value −4.77 dB at 10 GHz. The divider performance can be increased if the iris at port 3 is optimized in order to obtain a centered band ($L_{\text{iris}} = 12.5$, $w_{\text{iris}} = 11.46$) with a new matching network ($L_{m0} = 9.5$, $L_{m1} = 18$, $L_{m2} = 11.5$, $a_{m1} = 16.66$, $a_{m2} = 17.66$), as shown in Fig. 3b. In this case, the transmission band is 600 MHz again, but it is centered at 10 GHz, as required.

The previous example, even if not able to satisfy requirements, is important to understand how to enhance the performance of the divider. In fact, if we compare the electric field distribution in the empty divider, Fig. 3c, and the field in the divider with the iris, Fig. 3d, we can observe the presence of a null (dark blue) in the core of the divider near the third port and symmetrically placed. This null is the main effect of the iris placed at the third port which ensures that power is equally distributed to the output ports. It is evident that this electric field null can change its position and intensity by varying frequency. Hence, if a metallic septum is placed in the null zone, it ensures null of electric field at any frequency. At the same time, the iris can be removed, being useless for the presence of the septum. This placement permits to enhance divider performance by means of an optimization of the metallic septum position and dimension.

Following this approach, we try to optimize the core divider, i.e., the divider without the input matching network, to enlarge the transmission band, acting on the position and dimension of a metallic septum in symmetric position, in the absence of the iris at port 3, as shown in Fig. 4a. Hence, the goal is to obtain a quasi-flat transmission for $\left|S_{21}^{\text{core}}\right|$, $\left|S_{31}^{\text{core}}\right|$,

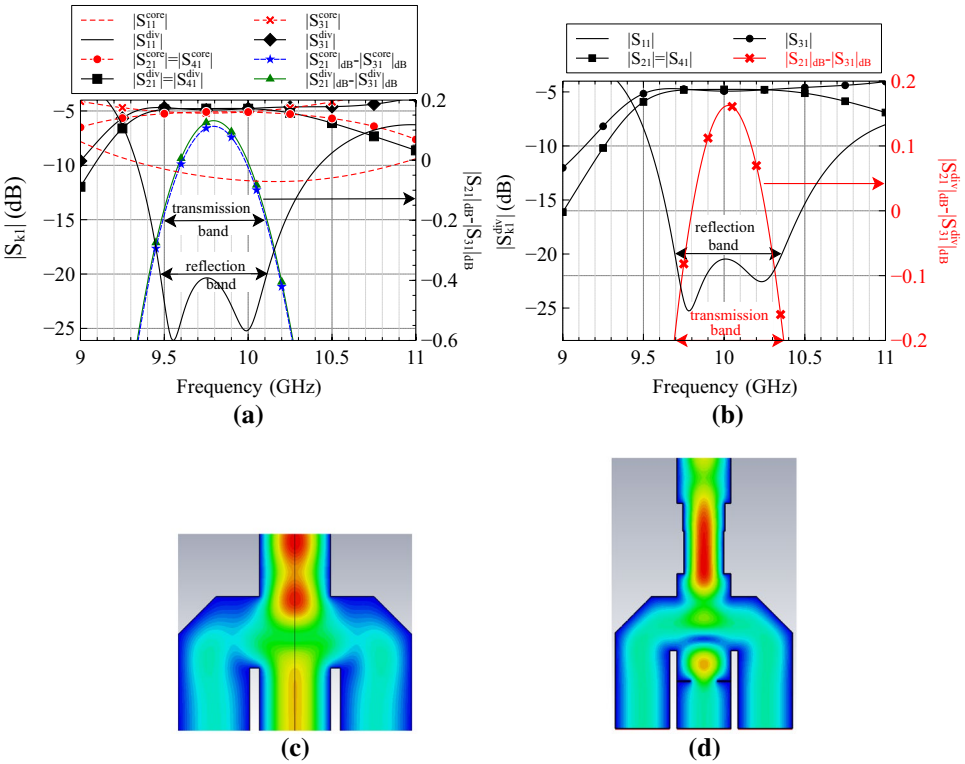

Fig. 3 Divider of Fig. 1 with iris at port 3. Scattering parameters amplitude $|S_{k1}|$ for excitation at port 1 (dimensions expressed in mm): **a** iris by (5); **b** iris optimized to center transmission band. **c** Electric field in the empty divider at $f = 10$ GHz; **d** electric field in the divider with iris at $f = 10$ GHz (Color figure online)

without optimization of $|S_{11}^{\text{core}}|$, over the required band 9.5 ÷ 10.5 GHz. In fact, while the global divider, made by matching network and divider core, must satisfy $|S_{21}^{\text{div}}|, |S_{31}^{\text{div}}| = -4.77\text{dB} \pm 0.1\text{dB}$ in the transmission band, the divider core constraint is that $|S_{21}^{\text{core}}|, |S_{31}^{\text{core}}|$ must be as flat as possible in the band. On the other hand, the matching network, designed in a successive step, must increase the values of $|S_{21}^{\text{div}}|, |S_{31}^{\text{div}}|$ to -4.77 ± 0.1 dB, with a difference between $|S_{21}^{\text{div}}|$ and $|S_{31}^{\text{div}}|$ in the range ± 0.2 dB.

Hence, in terms of optimization goal of the divider core, this requirement can be set as $-0.2 \le |S_{21}^{\text{core}}|_{\text{dB}} - |S_{31}^{\text{core}}|_{\text{dB}} \le 0.2$. This constraint should ensure that the design of a good matching network will force the transmission to $|S_{21}^{\text{div}}|, |S_{31}^{\text{div}}| = -4.77 \pm 0.1$ dB.

The electromagnetic analysis and optimization is obtained by the commercial software CST, and the obtained results are shown in Fig. 4b, for the optimized parameters $w_s = 4.28$, $L_s = 8.71$. The transmission band ($-0.2 \le |S_{21}^{\text{core}}|_{\text{dB}} - |S_{31}^{\text{core}}|_{\text{dB}} \le 0.2$) increases, with respect to the iris case, to about 800 MHz (9.57 GHz ÷ 10.33 GHz), with $|S_{11}^{\text{core}}| < -12$ dB. This result confirms that, replacing the null of electric field with a metallic septum, the transmission band of the divide core can increase. The following step is the design of a matching network at the input of port 1 to lower $|S_{11}^{\text{core}}|$ over the band and to increase $|S_{21}^{\text{core}}|, |S_{31}^{\text{core}}|$ to the

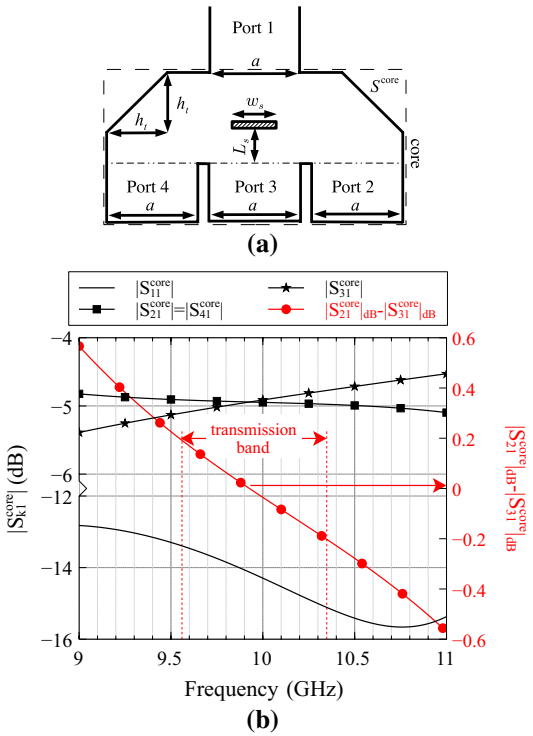

Fig. 4 **a** Divider core with central metallic septum. **b** Scattering parameters amplitude $|S_{k1}|$ for excitation at port 1 with $w_s = 4.28$ mm, $L_s = 8.71$ mm

desired value of -4.77 ± 0.1 dB. This design is omitted, at this moment, to try to further increase transmission band. To do this, the amplitude of the electric field in the divider core are shown in Fig. 5a–c at 9.5, 10 and 10.5 GHz, for an excitation at port 1.

Our intent is to observe where the electric field goes to zero (dark blue): this occurs symmetrically in the right/left part of the divider near port 2 and 4. These zones change their form with frequency as highlighted by the red arrows. As in the case of the electric field null due to the iris at port 3, we can try to add a metallic septum to enforce null of the electric field in these zones at any frequency. To do this, two lateral metallic septa of length w_p with thickness $t = 0.2$ are placed near ports 2 and 4, as shown in Fig. 6a, and a global optimization on h_t, w_s, L_s, w_p is performed with CST, obtaining: $h_t = 13.14, w_s = 3.94, L_s = 8.94, w_p = 3.94$. The amplitude of the scattering parameters for excitation at port 1 are shown in Fig. 6b for the core divider ($a = a_{m1} = a_{m2}$). $\left|S_{11}^{\text{core}}\right| < -16$ dB and the transmission band is greater than 2 GHz. These results show that the introduction of the lateral metallic septa where the electric vanishes is a good strategy to enforce vanishing of the electric field at any frequency, increasing transmission band. This is confirmed by the behavior of the electric field in Fig. 7a–c at 9.5 GHz, 10 GHz and 10.5 GHz: the distribution of the electric field is quite similar for the three analyzed frequencies.

The last step is the design of a matching network based on two optimized $\lambda_g/4$ transformers [17]. This design is not performed with CST to reduce computational time. In fact, the optimization with CST could require too many steps to converge to the best result in terms of matching network. Moreover, if the first matching stage is placed at a

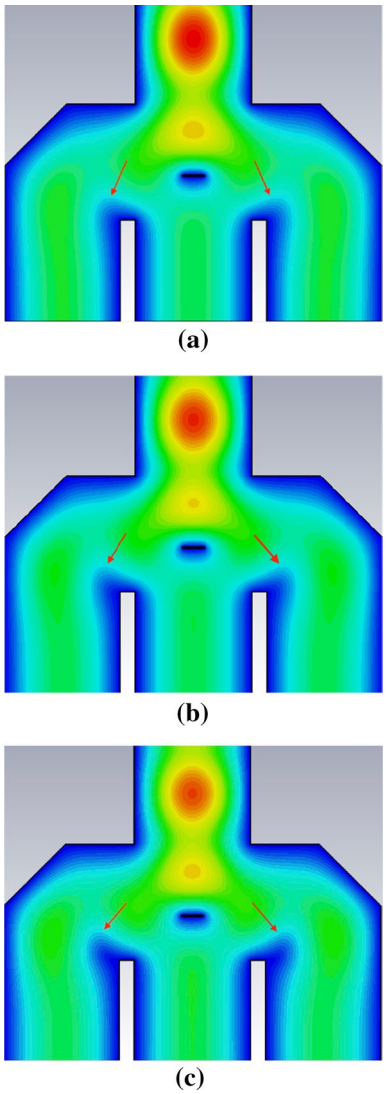

Fig. 5 Electric field of the core divider shown in Fig. 4a: **a** $f = 9.5$ GHz; **b** $f = 10$ GHz; **c** $f = 10.5$ GHz (Color figure online)

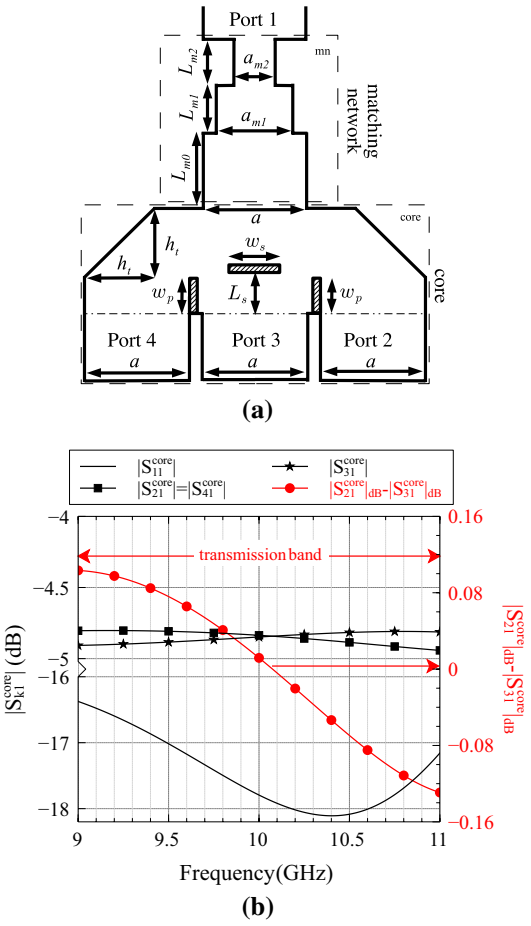

Fig. 6 **a** Divider with central and lateral metallic septa. **b** Scattering parameters amplitude $|S_{k1}|$ for excitation at port 1 for the core divider ($h_t = 13.14, w_s = 3.94, L_s = 8.94, w_p = 3.94, a = a_{m1} = a_{m2}$)

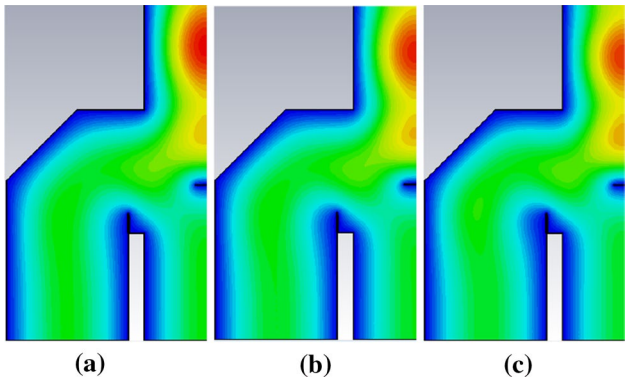

Fig. 7 Electric field of the core divider of Fig. 6b at: **a** $f = 9.5$ GHz, **b** $f = 10$ GHz, **c** $f = 10.5$ GHz

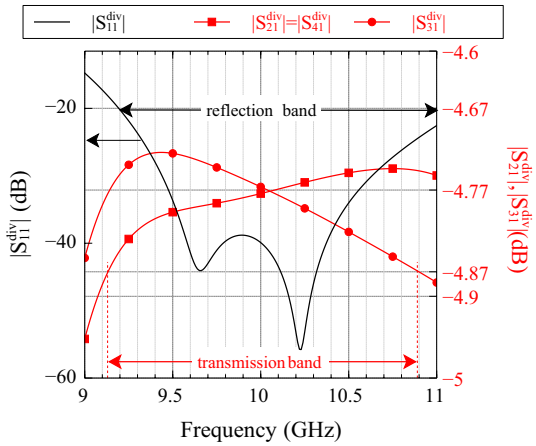

Fig. 8 Scattering parameters amplitude $|S_{k1}|$ for excitation at port 1 for the divider shown in Fig. 6a

proper distance L_{m0} from the input port of the divider core to neglect effect of higher order modes, as shown in Fig. 6a, the matching network does not alter the field distribution in the divider core or the transmission band, but lowers $|S_{11}|$ and increases $|S_{21}|, |S_{31}|$ to the desired values.

Hence, the matching network is designed evaluating at first the scattering matrix S^{core} at the input port of the unmatched divider core in the band of interest with CST.

Then, the transition between two waveguides with different width is evaluated with the MEN approach [18, 19], considering three accessible modes at the input and output ports, obtaining the 6x6 scattering matrix $S^{\text{wr}_1 \to \text{wr}_2}$. This analysis is needed to simulate the transition between the stages of the $\lambda_g/4$ transformers. Then, a database of the 6x6 scattering matrix $S^{\text{wr}_1 \to \text{wr}_2}$ is evaluated for different width in the range $18.86 \div 26.86$ mm (steps 0.1 mm). The database requires short computational time with a Fortran code (about 15 s for the full band for each transition). The database building is performed only one time, and it is used in the design of any matching network in the following of the paper. Finally, the possible combinations of the previous transitions separated by lengths L_{m0}, L_{m1}, L_{m2} are evaluated by cascading the relative scattering matrices $S^{\text{wr}_1 \to \text{wr}_2}$, shifted by the lines $j\beta_{10}L, \alpha_{30}L, \alpha_{50}L$, where $\beta_{10}, \alpha_{30}, \alpha_{50}$ correspond to the three propagating, or not, accessible modes and L to L_{m0}, L_{m1}, L_{m2}. The scattering matrix cascade of all combinations yields to a database of the scattering matrix of the matching network S^{mn} shown in Fig. 6a. The evaluation of the database of S^{mn} requires about ten minutes.

The last step is the choice of the best matching network S^{mn} for the scattering matrix of the divider core S^{core}. The reflection coefficient of the global divider (matching network and divider core) is obtained as combination of S^{mn} and S^{core}:

$$S_{11}^{\text{div}} = S_{11}^{\text{mn}} + \frac{S_{12}^{\text{mn}} S_{11}^{\text{core}} S_{21}^{\text{mn}}}{1 - S_{22}^{\text{mn}} S_{11}^{\text{core}}} \tag{7}$$

The choice of the best matching network is done starting from (7), using the database corresponding to all cases of matching network. The computation time is very fast (some minutes to obtain the best configuration for the matched divider).

This numerical matching technique is applied to the divider core of Fig. 6a, obtaining: $L_{m0} = 13.5$, $L_{m1} = 8$, $L_{m2} = 13.5$, $a_{m1} = 18.26$, $a_{m2} = 19.66$. The scattering coefficients of the matched divider are shown in Fig. 8: good matching is obtained over a reflection band of about 1.8 GHz. As expected, the matching network has not changed the difference $\left|S_{21}^{\text{div}}\right|_{\text{dB}} - \left|S_{31}^{\text{div}}\right|_{\text{dB}}$ with respect to Fig. 6b, but it has changed the actual values of $\left|S_{21}^{\text{div}}\right|, \left|S_{31}^{\text{div}}\right|$, obtaining a global transmission band that is related to the reflection band to maintain $\left|S_{21}^{\text{div}}\right|, \left|S_{31}^{\text{div}}\right|$ in the range -4.77 ± 0.1 dB as shown in Fig. 8. Hence, we can assume a global bandwidth of 1.8 GHz (9.1÷10.9) that is more than required.

Following the previous example, we can define an optimization procedure in three steps: first, an iris is placed at port 3 to equally share power among outputs and the electric field in the divider core is analyzed; second, the transmission to the output ports is optimized in the required band by placing proper metallic discontinuities in the position of the divider core where the electric field vanishes; third, a proper matching network is placed at the input port of the divider core to ensure low reflection in the required band. These three tasks are performed separately enhancing the optimization time. In fact, the first is based on a theoretical approach, while the other two tasks can be analyzed in two different phases being independent the two goals, as long as the transmission to the output ports is analyzed and insulation between ports is not taken into account.

A final remark must be done about the efficiency of the proposed approach. The bandwidth can be enlarged

by inserting some septa in the coupler, using an iterative approach, but it is not possible to evaluate *a priori* the maximum bandwidth that can be obtained. In fact, while the first two-three septa drastically alter the electromagnetic field of the empty device, the septa added at the successive steps can vary only some details of the global electromagnetic field, with a small increase of the bandwidth. Hence, the band enlargement tends to diminish with the number of septa/iterations.

If the isolation between ports must be taken into account in the design process, matching, power division and insulation must be taken into account at the same time. This approach is very complex as confirmed by the literature, showing that insulation is rarely included in the optimization.

The proposed approach is applied to the four-port star divider shown in Fig. 9a. The goal is to choose proper metallic septa to obtain 1 GHz transmission band centered at 10 GHz.

The first step is to put an iris at port 3, to understand where the first metallic septum must be placed, with the same approach previously discussed in (5) or (6). The chosen iris ($w_{\text{iris}} = 11.16$, $L_{\text{iris}} = 12.5$) yields to the results shown in Fig. 9b with black dashed line ($\left|S_{21}^{\text{core}}\right|$ "iris", left axis) and red continuos line ($\left|S_{21}^{\text{core}}\right|_{\text{dB}} - \left|S_{31}^{\text{core}}\right|_{\text{dB}}$ "iris", right axis). Analyzing the difference $\left|S_{21}^{\text{core}}\right|_{\text{dB}} - \left|S_{31}^{\text{core}}\right|_{\text{dB}}$, the divider core with the iris shows a transmission band of about 600 MHz (9.7÷ 10.3) and its electric field is shown in Fig. 10a. The field behavior suggests to place a central metallic septum (w_s, L_s) as done for the previous divider and shown in Fig. 9a, with $w_p = 0$.

The optimization of this septum ($w_s = 3.08, L_s = 3.78$) gives the result shown in Fig. 9b with black and red squared lines ("central"): the behavior of $\left|S_{21}^{\text{core}}\right|$ is more flat than the iris case and the transmission band ("tr. band. central" in the figure) is about 1.1 GHz, centered at 10 GHz. This divider core satisfies the requirements, but it is interesting to discuss the behavior of the electric field shown in Fig. 10b–d (only half divider core by symmetry). The field vanishes between ports 1 and 2 in an area that increases with frequency as highlighted by the arrows. In the previous divider, this occurred near port 3. This is due to the absence of the curved arms that, probably, forced the electric field to "curve" toward them.

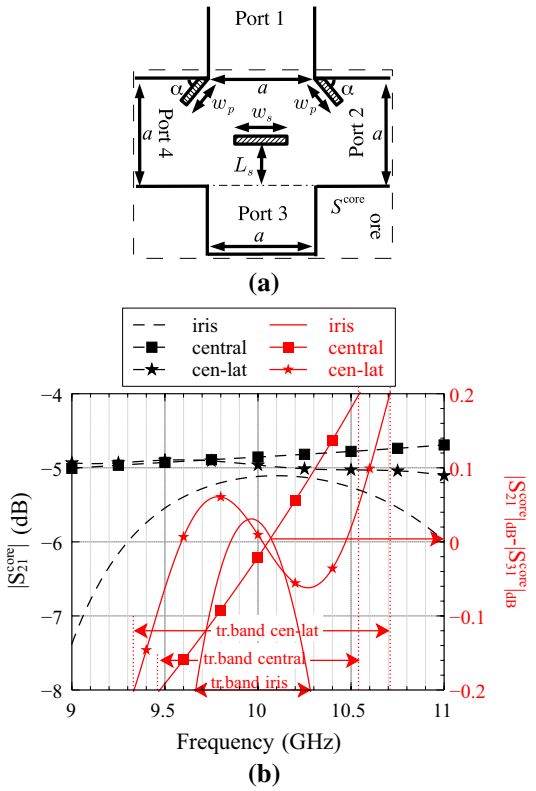

Fig. 9 **a** Star divider core. **b** Scattering parameters amplitude $|S_{21}|$ and $|S_{21}|_{\text{dB}} - |S_{31}|_{\text{dB}}$ for divider core (Color figure online)

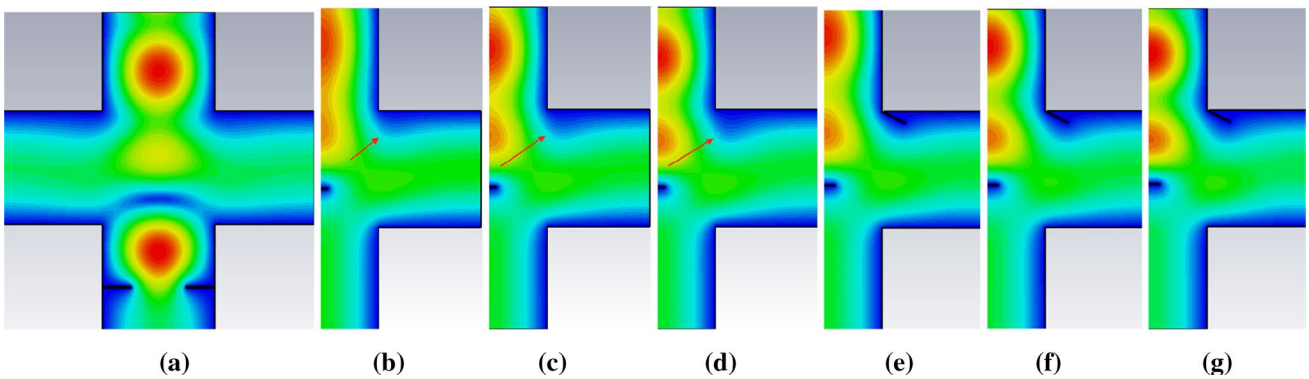

Fig. 10 **a** Electric field at 10 GHz for divider core with iris at port 3. **b–d** Electric field at 9.5, 10 and 10.5 GHz for divider core with central septum. **e–g** Electric field at 9.5, 10 and 10.5 GHz for divider core with lateral and central septa

To enforce the same field behavior at any frequency and to further enlarge bandwidth, we try to add two lateral metallic septa of length w_p at an angle α with respect to the metallic walls, as shown in Fig. 9a. The optimization of the geometric parameters of the lateral and central septa ($w_s = 4.28$, $L_s = 3.04$, $w_p = 4.99$, $\alpha = 63°$) yields to the results shown in Fig. 9b (black and red dashed starred lines, "cen-lat"). $\left|S_{21}^{\text{core}}\right|$ is more flat and the transmission band, measured on $-0.2 \le \left|S_{21}^{\text{core}}\right|_{\text{dB}} - \left|S_{31}^{\text{core}}\right|_{\text{dB}} \le 0.2$, increases to about 1.4 GHz ("tr. band. cen-lat" in the figure). Even in this case, the metallic septa placed in proximity of electric field null increase transmission band, and this is confirmed by the electric field behavior that is quite stable with frequency, as shown in Fig. 10e–g.

Now, we can design the matching network, as in Fig. 6a, to add to the input of port 1 of the star divider core ($L_{m0} = 14.5$, $L_{m1} = 8$, $L_{m2} = 15$, $a_{m1} = 17.86$, $a_{m2} = 19.06$) and the results are shown in Fig. 11a: reflection and transmission band (measured with respect to -4.77 ± 0.1 dB) give a global band of about 1.2 GHz. The transmission band measured as $-0.2 \le \left|S_{21}^{\text{div}}\right|_{\text{dB}} - \left|S_{31}^{\text{div}}\right|_{\text{dB}} \le 0.2$ is the same as the divider core case and is not altered by the matching network.

We can combine the star divider and the four-port divider previously designed to obtain a 2-stage 1:9 Beam Forming Network (BFN). This design can be done adding symmetrically a matched 90° bend to the star divider. If the bend is well matched in the band of interest, the star divider does not change its electromagnetic characteristics. To this purpose, we choose a 90° bend with $h_t = 14.806$ and the whole BFN is shown in Fig. 12a. A little offset between the external and internal connection lines between first and second stage of the BFN is needed to balance the effect of the bends in the external line ($L_{\text{ext}} = 14$, $L_{\text{int}} = 13$) with respect to the central line. The obtained scattering parameters for excitation at port 1 are shown in Fig. 12b. The obtained results satisfy the requirement on the transmission band, i.e., $|S_{k1}| = 10\log_{10}(1/9) = -9.54 \pm 0.1$ dB, with 1.05 GHz centered at 10 GHz.

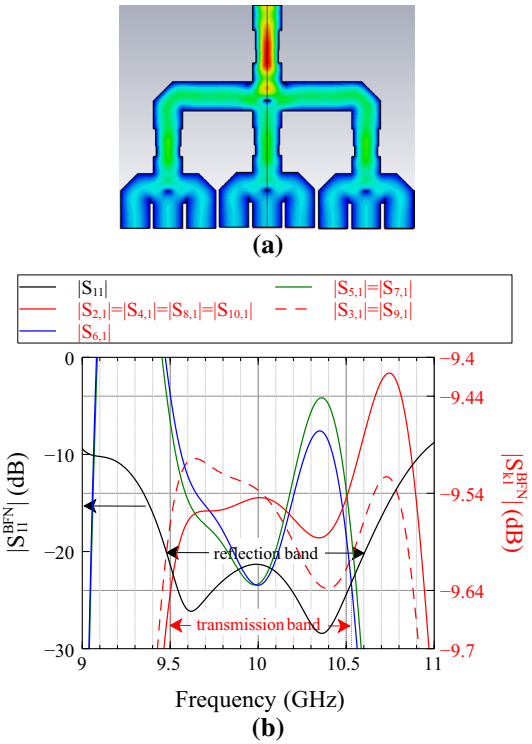

Fig. 12 **a** 1:9 BFN. **b** Scattering parameters amplitude $|S_{k1}|$ for excitation at port 1

There is a decrease in the bandwidth with respect to the bandwidth of the star divider (about 1.2 GHz) and the divider (about 1.9 GHz). In fact, it should be expected that the BFN bandwidth should be the same of the star divider, but this in not the case. This is due to the coupling between output ports of the star divider that alters the small recombinations of the waves reflected by the connections to the dividers, through the 90° bends. In fact, the coupling

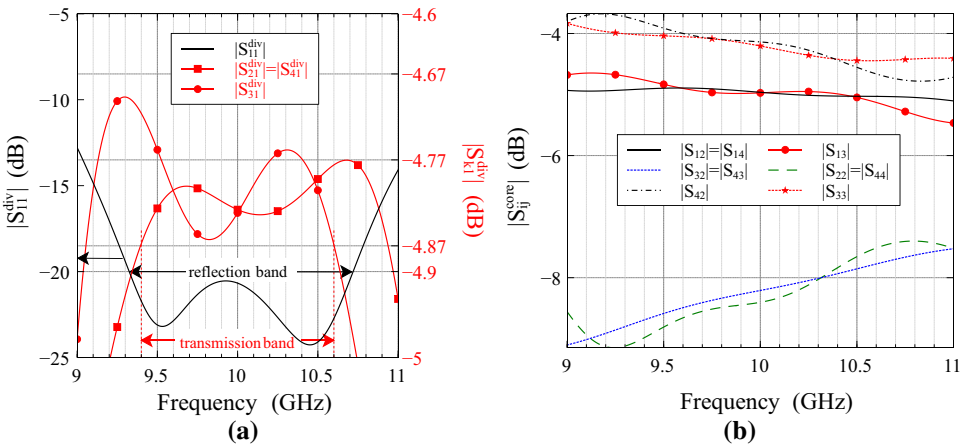

Fig. 11 **a** Scattering parameters amplitude $|S_{k1}|$ for matched star divider. **b** Coupling between ports for excitation at port 2, 3 and 4

between ports of the star divider connected to the bends is shown in Fig. 11b for excitation at port 2, 3 and 4. In an ideal divider [20], couplings between port 2 and ports 3, 4 are the same and, similarly, coupling between port 3 and ports 2, 4 are equal. For example, for a four-port divider, they are equal to 1/3, or −4.77 dB. This does not occur in the star divider, as shown in Fig. 11b, where the couplings are quite different. If all couplings be equal, the waves reflected by the second stage of the BFN were equally redirect toward other ports, without change of the global bandwidth of the BFN. In our case, the small reflections coming from the dividers at stage 2 come back to the star divider, and they are coupled between ports according to the scattering coefficients shown in Fig. 11b. Hence, a reduction of the transmission bandwidth occurs, from 1.4 GHz of the isolated star divider of Fig. 11a to 1.05 GHz of the BFN shown in Fig. 12b. Moreover, the effect of the non ideal insulation is that the input impedance of the BFN is slightly different from that of the insulated star divider. Hence, a new design of the BFN matching network is needed ($L_{m0} = 15, L_{m1} = 10, L_{m2} = 15, a_{m1} = 17.46, a_{m2} = 18.46$).

Another example is the design of the core of the 1:5 divider shown in Fig. 13. Even in this case, we must choose where proper metallic septa should be placed in the core to obtain a divider with 1 GHz bandwidth. First of all, we consider the empty divider, without lateral and central septa, and simulate it with CST, obtaining its scattering matrix S^{empty}. Then, as described in [16], we evaluate the susceptances and lines of the six-sides polygon that represents the divider. With simple mathematic/circuit manipulations, taking into account the symmetry of the device and similarly to the approach used for the four-port divider, we can synthesize the inductive irises to be placed at ports 3, 4 and 5, as shown in Fig. 14a, to obtain $|S_{21}| = |S_{31}| = |S_{41}| = |S_{51}| = |S_{61}|$.

The results are shown in Fig. 14b and even if $|S_{21}| = |S_{31}| = |S_{41}| = |S_{51}| = |S_{61}|$ at about 10 GHz, as required, the transmission bandwidth is less than 100 MHz. If we plot the electric field behavior in the empty divider with irises as shown in Fig. 14a, we observe the presence of two null of electric field, placed symmetrically, in each cavity of the divider core. Hence, we put two central metallic

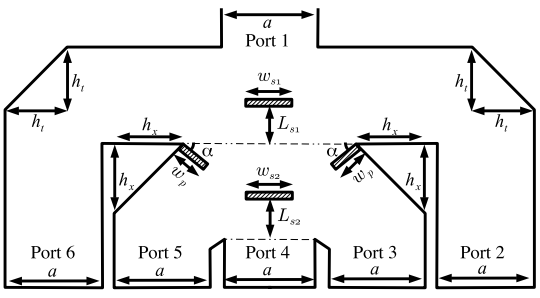

Fig. 13 1:5 divider core

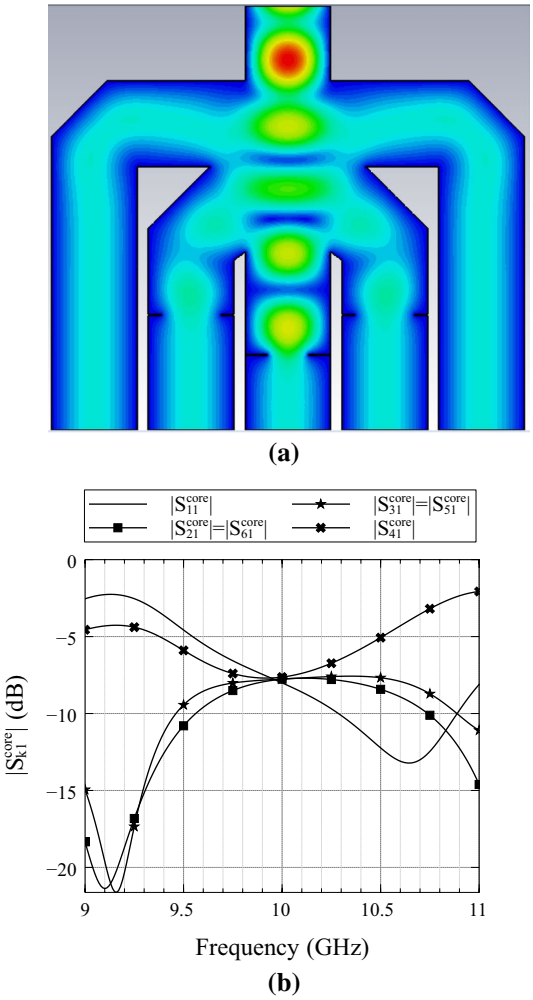

Fig. 14 **a** Electric field of 1:5 divider core with irises at ports 3, 4 and 5. **b** Scattering parameters $|S_{k1}|$ for excitation at port 1

septa as shown in Fig. 13 with $w_p = 0$ and optimize their positions and widths (L_{s1}, w_{s1}, L_{s2}, w_{s2}). The transmission band of the obtained results, not shown for brevity, increases to about 800 MHz and the electric field goes to zero near the edges between the two cavities and the extension of these areas changes with frequency. As done for the four-port divider, we put two lateral metallic septa near the edges to enforce null of electric field at any frequency, as shown in Fig. 13. The septa have dimension w_p and are placed at an angle α with respect to the edges. A global optimization on L_{s1}, w_{s1}, L_{s2}, w_{s2}, w_p, α, h_x is performed on the constraint $-0.2 \le \left|S_{k1}^{\text{core}}\right|_{\text{dB}} - \left|S_{n1}^{\text{core}}\right|_{\text{dB}} \le 0.2, k = 2, 3$ and $n = k + 1, 4$ yielding to a transmission band of about 1.2 GHz ($\alpha = 19°$, $h_t = 14.806, h_x = 16.55, L_{s1} = 1.58, L_{s2} = 8.89, w_{s1} = 1.55, w_{s2} = 4.62, w_p = 7.92$). Finally, a matching network at port 1 is designed ($L_{m0} = 11, L_{m1} = 13, L_{m2} = 20, a_{m1} = 24.66, a_{m2} = 20.86$), as in Fig. 6a, and the results for the global

divider are shown in Fig. 15a. The transmission band ($\left|S_{k1}^{\text{div}}\right| = 10\log_{10}(1/5) = -6.99 \pm 0.1$ dB) is about 1.2 GHz (9.4 ÷ 10.6), more than required, centered at 10 GHz and the reflection band is about 1.7 GHz, with a global bandwidth of about 1.2 GHz. The electric field at 9.5, 10 and 10.5 GHz is shown in Fig. 15b–d and is quite stable at any frequency. Hence, the proposed approach seems to give acceptable results.

The last examined structure is the star 1:5 divider core shown in Fig. 16a. Even in this case, the scattering matrix S^{empty} is evaluated and three irises are placed at port 3, 4 and 5, as previously done to ensure that $|S_{21}| = |S_{31}| = |S_{41}| = |S_{51}| = |S_{61}|$. The obtained transmission band is very small (here not reported for brevity), but, analyzing the null of the electric field, two central symmetrical septa are placed in the two cavities of the divider core. Then, the divider core with central septa is simulated and the electric field is analyzed. The transmission band

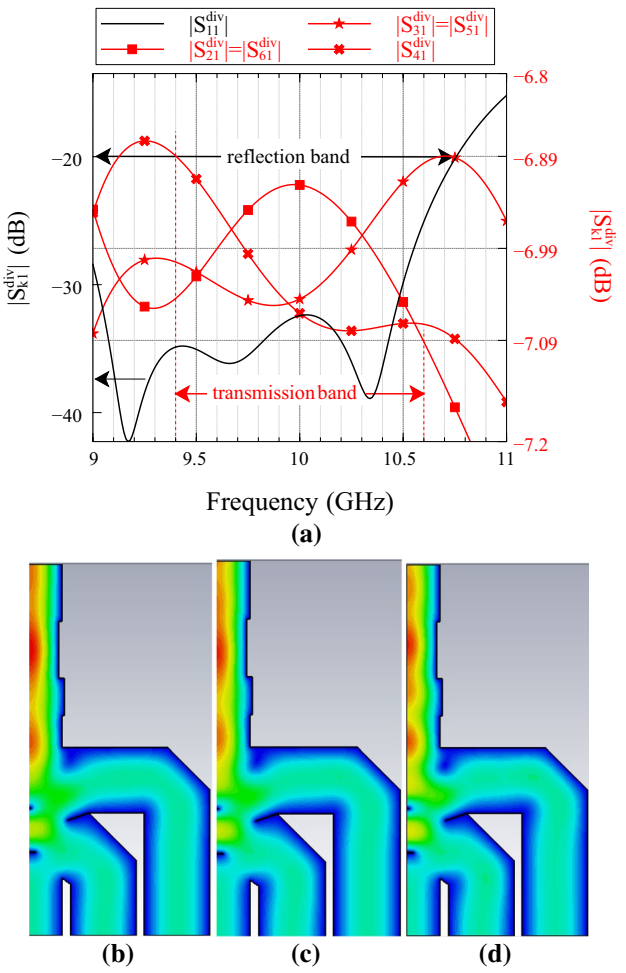

Fig. 15 **a** Scattering parameters $\left|S_{k1}\right|$ for excitation at port 1 of the matched 1:5 divider. **b–d** Electric field at 9.5, 10 and 10.5 GHz

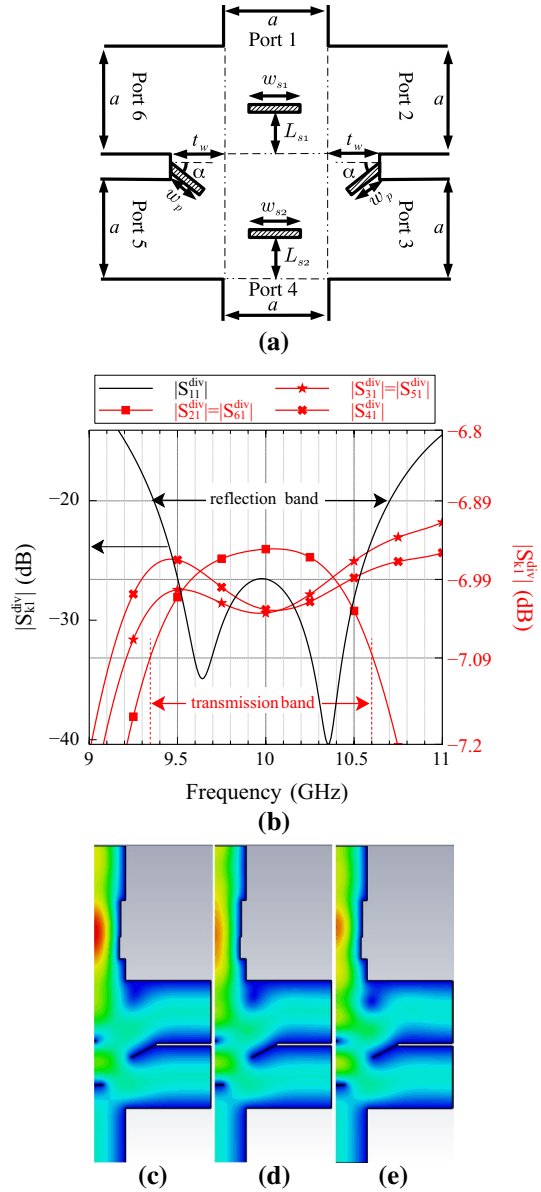

Fig. 16 **a** 1:5 star divider core. **b** Scattering parameters $\left|S_{k1}\right|$ for excitation at port 1 of the 1:5 star divider. **b–d** Electric field at 9.5, 10 and 10.5 GHz for the star divider with lateral and central septa

is larger than the case of the irises, but does not satisfy the requirement and, to enlarge it, two other lateral septa are placed at the border between the cavities where the electric field tends to vanish. Hence, an optimization on L_{s1},w_{s1}, L_{s2}, w_{s2}, w_p, α, t_w is performed with CST ($\alpha = 27°$, $L_{s1} = 1.02$, $L_{s2} = 8.74$, $w_{s1} = 1.28$, $w_{s2} = 6.56$, $w_p = 10.3$, $t_w = 11.18$), obtaining a transmission band of about 1.25 GHz (9.35 ÷ 10.6). Finally, the matching network is designed ($L_{m0} = 8$, $L_{m1} = 8$, $L_{m2} = 13.5$, $a_{m1} = 18.66$, $a_{m2} = 19.26$), and the results are shown in Fig. 16b. The electric field at 9.5, 10 and 10.5 GHz, Fig. 16c–e, shows that the behavior is quite stable varying frequency. Only

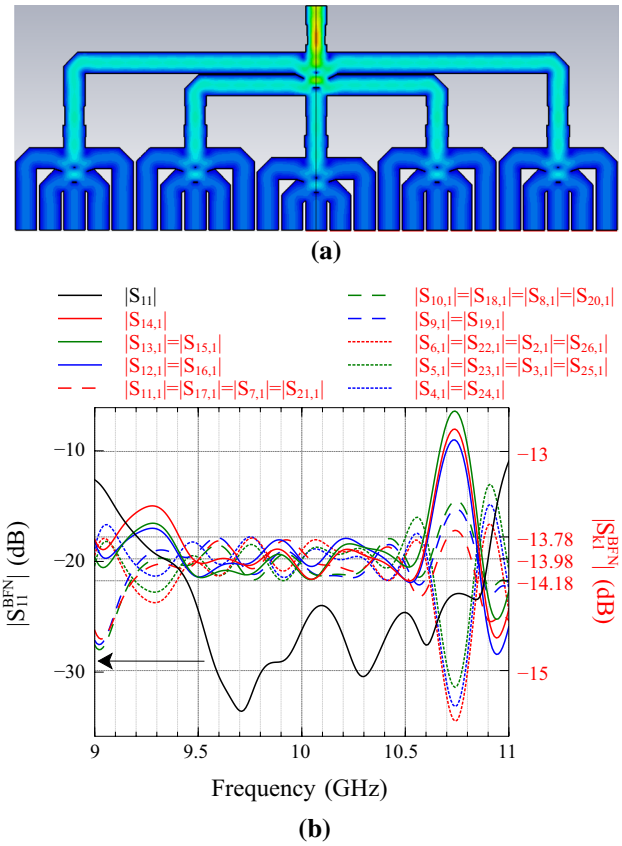

Fig. 17 **a** 1:25 BFN. **b** Scattering parameters amplitude $|S_{k1}|$ for excitation at port 1

in the first cavity, between ports 1 and 2, the electric field null changes its extension and form with frequency, and this fact could suggest to add two other lateral septa in that position to further enlarge transmission band. On the other hand, the required goals in terms of reflection and transmission band have been obtained without these new septa; hence, this further design is not performed.

These 1:5 dividers can be used to design a 1:25 BFN, as shown in Fig. 17a. The expected transmission band should be 1.2 GHz (9.4 ÷ 10.6), by the transmission band of the divider results shown in Figs. 15a and 16b. Unfortunately, the coupling between ports of the stage 1 divider reduces this band. To lower this effect, optimal choice of the length of the lines that connect stage 2 to stage 1 has been evaluated ($L_{\text{ext}} = 35, L_{\text{inner}} = 11, L_{\text{center}} = 22$), and a new input matching network must be designed ($L_{m0} = 8, L_{m1} = 9, L_{m2} = 12$, $a_{m1} = 19.06, a_{m2} = 19.66$). The global scattering coefficients of the BFN when port 1 is excited are shown in Fig. 17b. The transmission band requirement $\left|S_{k1}^{\text{div}}\right| = 10\log_{10}(1/25) = -13.98 \pm 0.1$ dB are not exactly satisfied by the BFN. Anyway, if we extend the limits to -13.98 ± 0.2dB, we obtain 1.1 GHz transmission band (9.4 ÷ 10.5). As pointed out before, this effect is due to the coupling between output divider ports.

3 Conclusion

A technique to design divider has been proposed, and it is based on the analysis of the electric field in the inner of the divider core. In fact, the initial design based on the insertion of irises at the output ports permits to identify where trial metallic septa can be placed in order to ensure that the electric field vanishes at any frequency. After an optimization of the septa, another analysis of the electric field gives the trial position of lateral metallic septa that could ensure an enlargement of the transmission band. A final optimization of the septa geometric parameters gives final transmission band that can satisfy the requirement. Finally, a matching network at the input port is designed to ensure that the transmission be at the desired value $10\log_{10}(\frac{1}{N})$, where N is the number of output ports.

Funding Open Access funding provided by Università Politecnica delle Marche.

References

1. Montgomery, C.G., Dicke, R.H., Purcell, E.M.: Principles of Microwave Circuits. McGraw-Hill (1948, I Ed.), Peter Peregrinus on behalf of the Institution of Electrical Engineers, London, U.K. (1987, II Ed.)
2. Marcuvitz, N.: Waveguide Handbook. Mc-Graw-Hill, New York (1951)
3. Wilkinson, E.J.: An n-way hybrid power divider. IRE Trans. Microw. Theory Tech. **8**(1), 116–118 (1960)
4. Holzman, E.L.: An eigenvalue equation analysis of a symmetrical coax line to n-way waveguide power divider. IEEE Trans. Microw. Theory Tech. **42**(7), 1162–1166 (1994)
5. Bialkowski, M.E., Waris, V.P.: Analysis of an n-way radial cavity divider with a coaxial central port and waveguide output ports. IEEE Trans. Microw. Theory Techn. **44**(11), 2010–2016 (1996)

6. Rozzi, T., Morini, A., Venanzoni, G., Farina, M.: Full-wave analysis of *N*-way power dividers by eigenvalue decomposition. IEEE Trans. Microw. Theory Tech. **57**(5), 1156–1162 (2009)
7. Ruiz-Cruz, J.A., Fahmi, M.M., Mansour, R.R.: Generalized multiport waveguide switches based on multiple short-circuit loads in power-divider junctions. IEEE Trans. Microw. Theory Tech. **59**(12), 3347–3355 (2011)
8. Chu, Q., Wu, Q., Mo, D.: A ka-band e-plane waveguide magic-t with coplanar arms. IEEE Trans. Microw. Theory Tech. **62**(11), 2673–2679 (2014)
9. Ding, J., Wang, Q., Zhang, Y., Wang, C.: A novel five-port waveguide power divider. IEEE Microw. Wirel. Compon. Lett. **24**(4), 224–226 (2014)
10. Cano, J.L., Mediavilla, A., Dragas, S., Tazon, A.: Novel broadband circular waveguide four-way power divider for dual polarization applications. IEEE Microw. Wirel. Compon. Lett. **26**(2), 98–100 (2016)
11. Farahbakhsh, A., Zarifi, D., Zaman, A.U.: 60-Ghz groove gap waveguide based wideband h-plane power dividers and transitions: for use in high-gain slot array antenna. IEEE Trans. Microw. Theory Tech. **65**(11), 4111–4121 (2017)
12. Arun Kumar, G., Biswas, B., Poddar, D.R.: A compact broadband riblet-type three-way power divider in rectangular waveguide. IEEE Microw. Wirel. Compon. Lett. **27**(2), 141–143 (2017)
13. Deng, J., Wang, Q., Zhao, P., Tian, M., Li, Q.: A quasi-planar *H*-plane waveguide power divider with full bandwidth. IEEE Microw. Wirel. Compon. Lett. **28**(8), 645–647 (2018)
14. Buesa-Zubiria, A., Esteban, J.: Design of five-way Bagley polygon power dividers in rectangular waveguide. IEEE Trans. Microw. Theory Tech. **66**(1), 116–127 (2018)
15. Zappelli, L.: Optimization procedure of four-port and six-port directional couplers based on polygon equivalent circuit. IEEE Trans. Microw. Theory Tech. **66**(10), 4471–4481 (2018)
16. Zappelli, L.: Simple, fast, and effective identification of an equivalent circuit of a waveguide junction with N ports. IEEE Trans. Microw. Theory Tech. **63**(1), 48–55 (2015)
17. Collin, R.E.: Foundations for Microwave Engineering, 2nd edn. The IEEE Press, New York (1992)
18. Zappelli, L.: Phased arrays of rectangular apertures on conformal cylindrical surfaces: a multimode equivalent network approach. IEEE Trans. Antenna Propag. **52**(7), 1843–1850 (2004)
19. Zappelli, L.: Multilayer array antennas with integrated frequency selective surfaces conformal to a circular cylindrical surface. IEEE Trans. Antenna Propag. **53**(6), 2020–2030 (2005)
20. Price, O.R., Leichter, M.: Scattering matrix for an n-port power-divider junction (correspondence). IRE Trans. Microw. Theory Tech. **8**(6), 669 (1960)